Materials Today Communications 38 (2024) 108222

Contents lists available at ScienceDirect

Materials Today Communications

journal homepage: www.elsevier.com/locate/mtcomm

An ab-initio study on the physical properties of double perovskite Cs_2AgXBr_6 (X=S, Te, Se)

Nabil Al-Aqtash [a,*], Anas Y. Al-Reyahi [a,*], Said Al Azar [b], Saber Saad Essaoud [c], Mufeed Maghrabi [a], Ahmad Mufleh [d], Mohammed Elamin Ketfi [e], Khadidja Berarma [f]

[a] Department of Physics, Faculty of Science, The Hashemite University, P. O. Box 330127, Zarqa 13133, Jordan
[b] Department of Physics, Faculty of Science, Zarqa University, Zarqa 13132, Jordan
[c] Department of Physics, Faculty of Science, University of M'sila, PO Box 166 Ichebilia, 28000 M'sila, Algeria
[d] Preparatory Deanship, Prince Sattam Bin Abdulaziz University, Al-Kharj, Saudi Arabia
[e] Department of Electronics, Faculty of Technology, University of M'sila, PO Box 166 Ichebilia, 28000 M'sila, Algeria
[f] Laboratory of Inorganic Materials, Department of Chemistry, University of M'sila, 28000 M'sila, Algeria

ARTICLE INFO

Keywords:
Semi-transparent metallic
DFT
Double perovskite
Optoelectronic

ABSTRACT

Cs_2AgXBr_6 (X = S, Se, and Te) double perovskite structural, electronic, and optical properties were investigated using the density functional theory (DFT) method combined with various correlation potentials such as TB-mBJ, LDA, PBE, WC, and hybrid functionals (YS-PBE0). The calculated structural and elastic properties revealed that the Cs_2AgXBr_6 compounds are elastically stable, ductile, anisotropic, and ionically bonded. Both Poisson ratio and Pugh ratio confirm that Cs_2AgXBr_6 (X = S, Te, Se) compounds are ductile. The calculated density of States (DOS) and the electronic band structures of the investigated compounds display zero band gaps for these compounds. Therefore, the calculated electronic properties of these compounds indicate their metallic nature. The calculated optical transmittance shows the transparent behaviors of studied compounds.

1. Introduction

perovskite compounds have been studied for their intriguing properties, including superconductivity, insulating, metallic, or semi-metallic behavior, and magnetic activity that spans from antiferromagnetic to ferromagnetic. Their properties make them excellent candidates for several applications [1,2].

The perfect cubic perovskite ABX_3 normally has twelve large cations of element A, one smaller cation at site B, and an anion of element X, commonly chalcogenide or halide. However, double perovskite consists of two groups of ABX_3 creating $A_2B_2O_6$, where one B is altered to a B′, resulting in $A_2BB'O_6$. Double perovskite compounds with two separate transition metal elements at B sites (B, B′) and two distinct rare-earth and alkaline earth elements at A allow for more innovation than simple perovskites with one A and one B cation site. The formula for (doubly ordered perovskite) or (double-double perovskite) is $AA'BB'O_6$ [3–7].

High charge carrier density gives perovskite halide compounds a 28 % power conversion efficiency (PCE) [8,9]. Their light-gathering efficiency makes them suitable for an active layer in single-junction photovoltaic cells. Perovskite and double perovskites have been investigated as possible solar cell materials [10]. The $Cs_2AgBiBr_6$ structure is an inorganic double perovskite system that could replace solar cells. $Cs_2AgBiBr_6$ was synthesized and structurally analyzed [11,12]. The non-toxic Pb-free $Cs_2AgBiBr_6$ has well-visible spectrum light absorption and optical stability in air and humidity [13,14]. Its band gap makes it suitable for photovoltaic and X-ray detectors [15–17].

Substantial theoretical investigations focused on changing specific atoms in $Cs_2AgBiBr_6$ to generate compounds with similar or superior characteristics for use in various industries. W. Li *et al.* reported that $Cs_2AgBiBr_6$ is an excellent material for optoelectronics and photovoltaics due to its toughness, low thermal expansion, high thermal moisture durability, and nontoxicity [17]. According to a study by McClure *et al.*, $Cs_2AgBiBr_6$ and $Cs_2AgBiCl_6$ remain stable in the air [18]. The optical, electronic, mechanical, structural, and thermal properties of Cs_2ZSbX_6, where Z = Ag, Cu, and X = Cl, Br, and I, were investigated by Soni *et al.* [19]. Such compounds can be used in optoelectronics due to their optical activity in the visible and ultraviolet ranges. Wang *et al.* show that the energy bandgap of $Cs_2AgBiBr_6$ can be tuned by Cl-doping, which is useful for its potential application in optoelectronic devices [20]. The theoretical efforts to study the generated compounds from $Cs_2AgBiBr_6$

* Corresponding authors.
E-mail addresses: nabild@hu.edu.jo (N. Al-Aqtash), anasy@hu.edu.jo (A.Y. Al-Reyahi).

https://doi.org/10.1016/j.mtcomm.2024.108222
Received 11 December 2023; Received in revised form 20 January 2024; Accepted 25 January 2024
Available online 1 February 2024

are still going on for a better understanding of these new compounds.

In this work, we explored the Cs_2AgXBr_6 (X = S, Te, and Se) compounds using the density functional theory (DFT) with several exchange potentials (PBE, LDA, mBJ, and hf). The structural, electronic, and optical properties of these compounds were investigated. The importance of this study lies in determining the physical characteristics of these compounds, evaluating them in comparison to other compounds with similar characteristics, and extrapolating the uses of these compounds based on the obtained results.

2. Computational details

The structural, electronic, and optical parameter calculations of Cs_2AgXBr_6 (X = S, Te, and Se) compounds were performed using the full-potential linearized augmented plane wave (FP-LAPW) method within DFT accompanied by Wien2k [21–27].

Electronic properties like the dispersion curve and density of states can be computed with various approximations, such as local density approximation (LDA) and generalized gradient approximation (GGA) [28–31]. However, these approximations underestimate the bandgap of rock salt structures. Even though hybrid functionals have been utilized as magnificent and appropriate approximations as an exchange-correlation potential [32,33]. In contrast, their high computational costs yet urge us to shift towards another approximation. The Becke-Johnson (BJ) potential has evolved into a unique form that is known as the Tran-Blaha modified Becke-Johnson (TB-mBJ). This updated model reproduces the Kohn-Sham (KS) potential exactly and gives the most accurate way of computing the bandgap [34,35]. Yet, the hybrid functionals (hf) method is the one that yields the most accurate results for calculating the bandgap. The fourth rung on Jacob's ladder corresponds to the hybrid functionals that Wien2k constructed, and these hybrid functionals can either be unscreened or screened. It was demonstrated that the outcomes from the error function-based screened hybrid functionals are extremely similar to the outcomes from the screening of the Coulomb operator utilizing exponential function in screened hybrid functionals. This was accomplished by carefully selecting the screening parameter (YS-PBE0) [32,33].

Therefore, Several DFT approximations, such as the local density approximation (LDA), generalized gradient approximation (GGA), meta-GGA, occupied orbitals, and unoccupied orbitals, have been used in this work to calculate the various physical properties of Cs_2AgXBr_6 compounds. The GGA is used in more up-to-date implementations of DFT, and it improves upon LDA by integrating extra electron density requirements for maintaining high accuracy. These criteria include the Perdew-Burke-Ernzerhof (PBE), Modified Becke and Johnson (mBJ), and complete hybrid functionals (hf). Jacob's ladder is built one step at a time by extending the potential into a series of words. In the first term, electron density determines the LDA, and in the second term, the first derivative determines the GGA, the LDA, and GGA make up the first two rungs. Radii measured in muffin tins (R_{MT}) were uniformly set for all atoms to be 2.5. So far, $R_{MT}\times K_{max}$ was considered to be 8, which is the dimension of the matrix that has been defined. With a cutoff of −6.0 Ry, the energy was carefully calibrated. The maximum charge density is raised to $G_{max} = 14\ (a.u.)^{-1}$ by use of the Fourier series. Integration over the Brillouin zone was performed with k-points of 15 × 15 × 15 [36,37]. The unit cell must be changed to eliminate strain at the ground state to compute the total energy in terms of volume, and then plug that energy into Murnaghan's equation to determine the parameters and characteristics of the composition at the ground state [29,30]. However, the compounds' spin up and down are equal, therefore the attributes of the structures might be computed without taking the spin into account.

The heat capacities of the three compounds under examination were determined utilizing the Debye quasi-harmonic model, which is integrated into the GIBBS2 software. The present analysis was performed under diverse pressure conditions, ranging up to 15 gigapascals (GPa), and within a temperature interval of up to 650 Kelvin (K).

3. Results and discussion

3.1. Structural and elastic properties

The structural characteristics of the cubic double Perovskite Cs_2AgXBr_6 (X = S, Te, Se) in the *Fm-3m* (#225) space group were investigated [19]. The unit cell of these structures is illustrated in Fig. 1. The Murnaghan formula of state (Eq. 1) was used to determine equilibrium lattice parameters, bulk modulus, and pressure derivative to optimize the structure.

$$E(V) = E_0 + \frac{B_0 V}{B_0'}\left[\frac{(V_0/V)^{B_0'}}{B_0'} + 1\right] - \frac{B_0 V}{B_0' - 1} \quad (1)$$

Where B_0 and B'_0 are the equilibrium bulk modulus and its derivative.

Fig. 2 shows the total energy versus unit cell volume graph [36,38,39]. The relaxed volume represented in the energy-volume parabola at the minimum energy for Cs_2AgXBr_6 is obtained by varying the unit cell volume over the equilibrium volume while computing the total energy. Furthermore, Table 1 lists the calculated minimum volume, lattice parameter, and bulk modulus of Cs_2AgXBr_6 structures with different energy exchange, where the Bulk modulus (B) reflects how the material behaves under uniform strain [36].

Furthermore, the stability of the compounds was assessed by employing the principles of cohesive energy and formation energy. The cohesive energy (E_{coh}) was determined using the equation: $E_{coh} = (2E_{Cs} + E_{Ag} + E_x + 6E_{Br} - E_{tot})/40$. In this equation, E_{tot} represents the total bulk energy of Cs_2AgXBr_6 compounds, while E_{Cs}, E_{Ag}, E_x, and E_{Br} represent the total energies of the isolated Cs, Ag, X, and Br atoms, respectively. In contrast, the calculation of the formation energy (E_{from}) was conducted using the following formula: $E_{form} = E_{tot} - (2E_{Cs} + E_{Ag} + E_x + 6E_{Br})/40$. Here, E_{tot} represents the overall bulk energy of Cs_2AgXBr_6 compounds, while E_{Cs}, E_{Ag}, E_x, and E_{Br} denote the total energies of the Cs, Ag, X, and Br atoms in their respective most stable bulk configurations.

The values of E_{coh} and E_{form}, as determined through calculations, are presented in Table 1. According to the provided equations, a material is considered stable when the E_{coh} value is positive and the E_{form} value is negative. The cohesive energies of Cs_2AgXBr_6 (where X represents S, Se, and Te) were determined to be 3.886, 3.643, and 3.593 eV/atom, respectively. The positive values of the E_{coh} obtained from the investigation suggest that the compounds exhibit chemical stability. In the same way, the formation energy (E_{form}) of Cs_2AgXBr_6 (where X represents S, Se, and Te) has been determined to −1.554, −1.440, and −1.432 eV/atom, respectively. The negative formation energy ensures these compounds are thermodynamically stable [40,41].

Dynamic stability analysis was conducted by calculating phonon frequency modes at the Γ point using VASP package [42–44] and finite

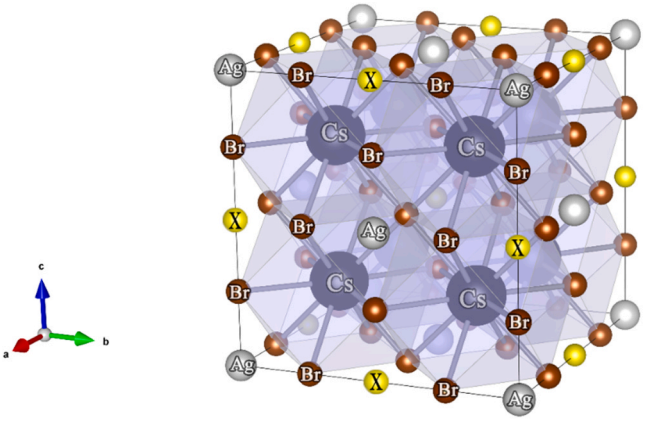

Fig. 1. The unit cell of the cubic double Perovskite Cs_2AgXBr_6.

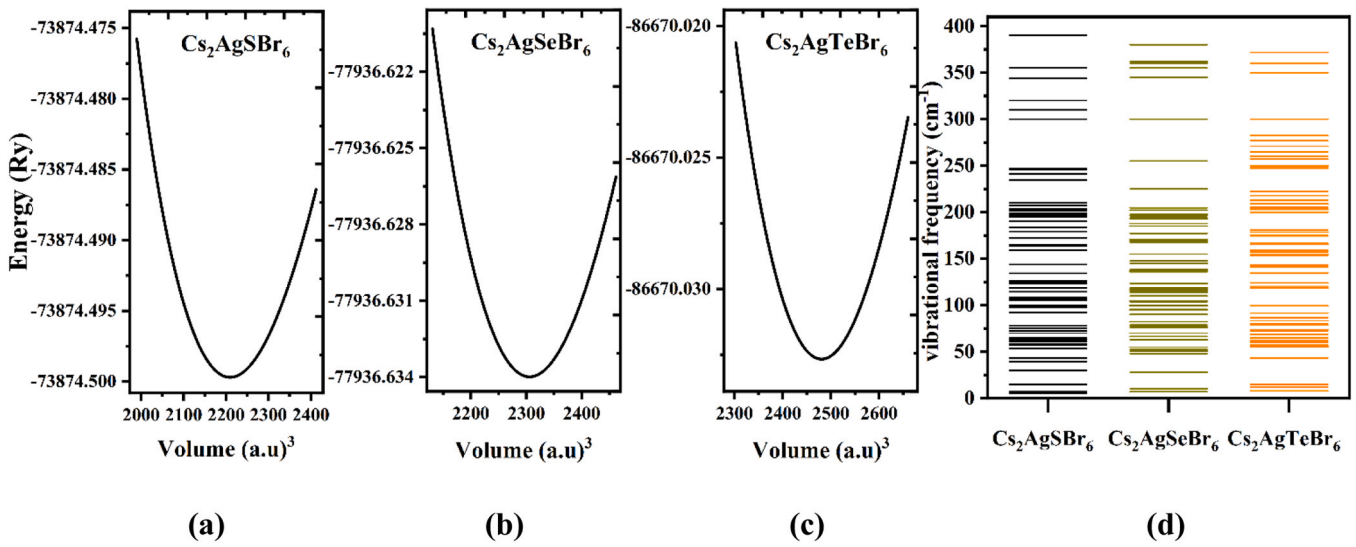

Fig. 2. The PBE energy exchange volume-energy graph for Cs_2AgXBr_6 structures where **(a)** X = S, **(b)** X = Se, and **(c)** = Te, and (d) the vibrational frequencies (3 N–6) of the lowest energy Cs_2AgXBr_6 structures.

Table 1
The calculated lattice parameter and bulk modulus of Cs_2AgXBr_6 structures with different energy exchange, as well as, the cohesive and formation energies in (eV/atom).

	Cs_2AgSBr_6	$Cs_2AgSeBr_6$	$Cs_2AgTeBr_6$
a(Å) – PBE	10.94	11.10	11.37
a(Å) – LDA	10.43	10.76	10.95
a(Å) – WC	11.05	11.15	11.57
V_0 (a.u)^3 – PBE	2209.58	2305.96	2480.79
B (GPa)	25.3613	25.3224	23.8755
E_{coh} (eV/atom)	3.886	3.643	3.593
E_{form} (eV/atom)	-1.554	-1.440	-1.432

differences methods. Fig. 2d shows that the vibrational frequencies of the lowest energy structures of Cs_2AgXBr_6 are all positive and have no imaginary components. This means all compounds are stable.

C_{11}, C_{12}, and C_{44}, known as the elastic constants, were investigated using the exchange-correlation potential of LDA and (GGA-PBE) at 0 K and 0 Gpa to deduce the mechanical properties of the materials and predict the influence of an external force on a crystal. Eqs. 2, 3, and 4 provide the three generally acknowledged conditions for the elastic stability of cubic crystals [45].

$$C_{11} + 2C_{12} > 0 \quad (2)$$

$$C_{44} > 0 \quad (3)$$

$$C_{11} - C_{12} > 0 \quad (4)$$

Calculating the elastic constants determines the crystal's response to external forces. The elastic constants indicate the solid's stability, hardness, brittleness, asymmetry, bonding nature, and elastic wave propagation mode. The elastic characteristics of cubic double Perovskite Cs_2AgXBr_6 compounds can be predicted using C_{11}, C_{12}, and C_{44} elastic constants [46]. The Cauchy pressure relation ($C_P = C_{12} - C_{44}$) was used to predict the solid material atom bonding [47]. Positive values endorse ionic bonding, while negative values endorse covalent bonding. Table 2 lists the calculated elastic constants (C_{11}, C_{12}, and C_{44}) and Cauchy pressure (C_P) for the Cs_2AgXBr_6 compounds. Cauchy pressure values, shown in Table 2, indicate that the ionic bonding is dominant in these compounds.

Table 2
The elastic constants (C_{11}, C_{12}, and C_{44}) and Cauchy pressure (C_P) in Gpa.

	C_{11}	C_{12}	C_{44}	C_p=C_{12}-C_{44}
Cs_2AgSBr_6	51.56	16.51	12.80	3.71
$Cs_2AgSeBr_6$	42.67	15.66	8.03	7.63
$Cs_2AgTeBr_6$	43.71	14.39	5.43	8.96

Bulk modulus (B), shear modulus (G), Young modulus (Y), and Poisson's ratio (ν) of the investigated compounds, as listed in Table 3, are obtained from the predicted elastic constants using the averaging approach of Voigt, Reuss, and Hill (VRH) [48]. The Poisson ratio (ν) is also crucial to understand the type of bonding. Brittle or ductile solids are classified by the Poisson ratio of 0.26. A material is ductile if its value is greater than the threshold and brittle if it is less [49–51]. The Poisson ratio is greater than 0.26, indicating that all compounds investigated are ductile. Another important statistic is indeed the Pugh ratio (B/G), which predicts brittle and ductile properties. The material is ductile until B/G is more than 1.75 [26,52]. Therefore, both Poisson ratio and Pugh ratio reveal that Cs_2AgXBr_6 (X = S, Te, Se) compounds are ductile.

Anisotropy (A) affects micro-crack transmission and structural stability. Crystalline materials exhibit elastic anisotropy if A deviates from 1, where $A = \frac{2C_{44}}{C_{11}-C_{12}}$ [46,53]. Our results show that all investigated compounds are anisotropic. Crystalline solids' Debye temperature (θ_D) relates elastic properties with thermodynamic parameters such as specific heat, vibrational entropy, and melting temperature [46]. This is estimated by averaging the sound velocity of elastic wave velocities throughout multiple crystal directions using Eq. 5 and 6.

Table 3
The estimated Bulk (B), Shear (G), Young's modulus (Y), Poisson ratio (ν), anisotropic (A), Pugh's index (B/G), Debye Temperature (θ_D), transverse velocity (ν_t), longitudinal (ν_l), and average elastic sound velocity (ν_m) for Cs_2AgXBr_6 structures.

	Cs_2AgSBr_6	$Cs_2AgSeBr_6$	$Cs_2AgTeBr_6$
B (Gpa)	28.193	24.667	24.164
G (Gpa)	14.518	9.904	8.190
Y (Gpa)	37.173	26.204	22.075
ν	0.280	0.322	0.347
A	0.730	0.595	0.370
B/G	1.942	2.491	2.950
θ_D (K)	186.472	151.985	136.839
ν_t (m/s)	1798.28	1478.69	1359.69
ν_l (m/s)	3254.48	2891.56	2814.19
ν_m (m/s)	2003.7	1656.55	1528.26

$$\theta_D = \frac{h}{k_B}\left[\frac{3n}{4\pi}\left(\frac{N_A\rho}{M}\right)\right]^{\frac{1}{3}} \quad \nu_m \tag{5}$$

$$\nu_m = \left[\frac{1}{3}\left(\frac{2}{\nu_s^3}+\frac{1}{\nu_l^3}\right)\right]^{-\frac{1}{3}}, \nu_l = \left[\frac{B+\frac{4G}{3}}{\rho}\right]^{\frac{1}{2}}, \text{and} \nu_s = \left[\frac{G}{\rho}\right]^{\frac{1}{2}} \tag{6}$$

Where ν_m is the mean sound speed, ρ is the mass density, h is Planck's constant, k_B is Boltzmann's constant, B is the bulk modulus, N_A is Avogadro number, G is the shear modulus, n is the number of atoms per formula unit, and M is the molecular weight. Nonetheless, d is a rough estimate of a solid's Debye hardness. The calculated data in Table 3 show that Cs_2AgSBr_6 is the hardest and $Cs_2AgTeBr_6$ is the softest.

3.2. Electronic properties

The total density of states (TDOS) for the Cs_2AgXBi_6 sets of double perovskites is virtually similar due to the analogous framework of the structure formed by $A_2ZZ'X_6$ composition. The range −6 eV to 0 eV below the Fermi level represents the occupied energy states and the range 0 eV– 6 eV above the Fermi level represents the unoccupied energy states as depicted in Fig. 3, where the Fermi level sets to 0 eV as a reference level. As shown in Fig. 3, there is no bandgap due to the overlap between the conduction band and the valence band.

Partial density of states (PDOS) has also been calculated, as shown in Fig. 4, for sub atoms such as Cs, Ag, Br and X = (S, Se, Te) to get detailed information concerning the hybridization. The density of states in the upper conduction band crossing fermi level to the lower valence band is due to the p orbital of the chalcogen atoms (X). PDOS show that the p shell of the X = (S, Te, Se) is primarily responsible for the overlap of the conduction and valence bands. Nonetheless, the largest contributors to the conduction band are the s-shell from Cs and the p-shell from Br. These compounds show metallic behavior due to this overlapping between the conduction band and the valence band electrons.

Moreover, Fig. 5 depicts the electronic band structures of the investigated Cs_2AgXBi_6 compounds over the energy range from - 6 to 10 eV in the high symmetry directions. The band structures were calculated using the first Brillouin's high symmetry point at 0 GPa and 0 K, TDOS, and PDOS. Nevertheless, the exchange-correlation potential for Cs_2AgXBi_6 was evaluated using TB-mBJ and PBE, WC, LDA, and hf (YS-PBE0) energy exchange-correlation. Since the upper and lower spins are symmetrical, the bandgap was determined without considering the spin. The obvious conclusion that can be drawn from Fig. 5 is that the band gap value for these compounds is zero, indicating that they behave like metals.

3.3. Optical properties

The optical characteristics of the compounds were investigated using the hybrid functional (YS-PBE0). Complex dielectric function $\varepsilon(\omega)$, complex optical conductivity $\sigma(\omega)$, complex refractive index $n(\omega)$, extinction coefficient $k(\omega)$, absorption coefficient $I(\omega)$, and energy loss $L(\omega)$ [23,24,26,27,36,54] of the Cs_2AgXBr_6 compounds have been investigated in the energy range 0 to 13 eV by employing the Kramers-Kronig transformation. The remaining optical properties were determined using the equations mentioned by Al-Reyahi *et al.* [37]. only one tensor component is required because of the symmetry of its cubic crystal structure ($\varepsilon_{xx} = \varepsilon_{yy} = \varepsilon_{zz}$).

A medium's optical response to incident photon energy is represented by both real $\varepsilon_1(\omega)$and imaginary$\varepsilon_2(\omega)$ dielectric function $\varepsilon(\omega) = \varepsilon_1(\omega) + i\varepsilon_2(\omega)$. Both components are related to dispersive and absorptive behavior, respectively. All the principal peaks of the optical spectra are distinctive when plotting the real and imaginary parts of the complex dielectric function against the incident radiation energy [55].

Fig. 6 depicts that ε_1 starts from the negative value at the zero energy, then the behavior of ε_1 tends to increase rapidly to reach the maximum at 0.96, 1.17, and 1.93 eV for Cs_2AgSBr_6, $Cs_2AgSeBr_6$, and $Cs_2AgTeBr_6$ respectively. However, the $Cs_2AgSeBr_6$ peak is the smallest among all of them. It then tends to decrease rapidly to reach the negative in the range (1.23–4.51), (1.13–3.56), and (1.17–3.56) eV for the same compound arrangement. Cs_2AgSBr_6 also exhibits a second negative region between 7.19 and 8.23 eV. A second peak occurs at around 6.02, 7.87, and 6.70 eV for the compounds before they gradually drop and go back to the negative value again. In addition, Fig. 6 (illustrates ε_2 versus the photon energy) reveals that for Cs_2AgXBr_6, ε_2 has a very high positive value at 0 eV and rapidly decreases then goes back to increase to around 1 eV. After achieving peak values at 1.12, 1.38, and 2.58 eV for Cs_2AgXBr_6 (X = S, Se, and Te), ε_2 progressively dropped. However, the major peak of $Cs_2AgTeBr_6$ is the shortest.

The material acts metallically whereas ε_1 is positive, otherwise, it acts like a semiconductor [56]. In addition, the Debye model, and the concept of permittivity (where D and E are the amplitudes of the displacement vector and the electric field vector, respectively) provide insight into the significance of the negative value of ε_1. The connection between D and E at a given frequency is described by the permittivity tensor $\varepsilon = D/E$. When ε_1 is positive, D and E point in the same direction; when it is negative, they become perpendicular. It is worth noting that most dielectrics have positive permittivity values [57]. Considering the preceding discussion, the negative value of ε_1 in the aforementioned

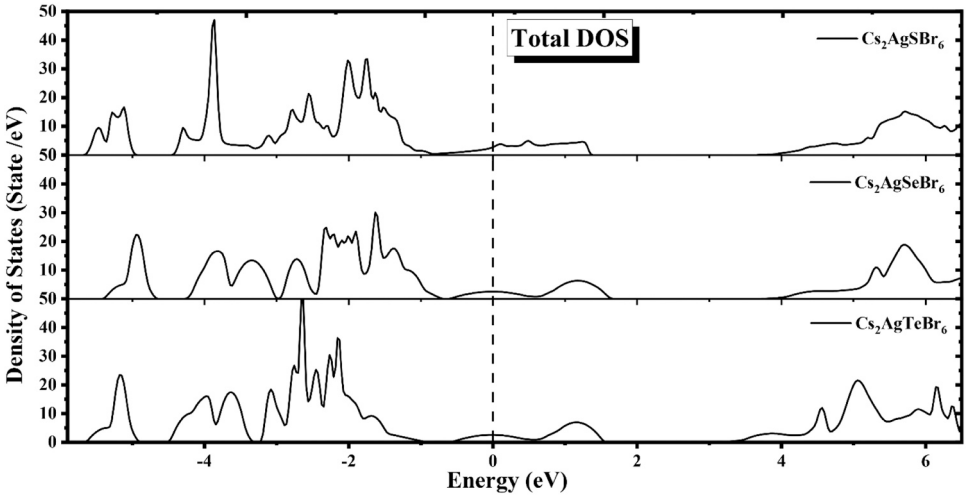

Fig. 3. The total density of states (TDOS) of Cs_2AgXBi_6 compounds (X = S, Se, Te).

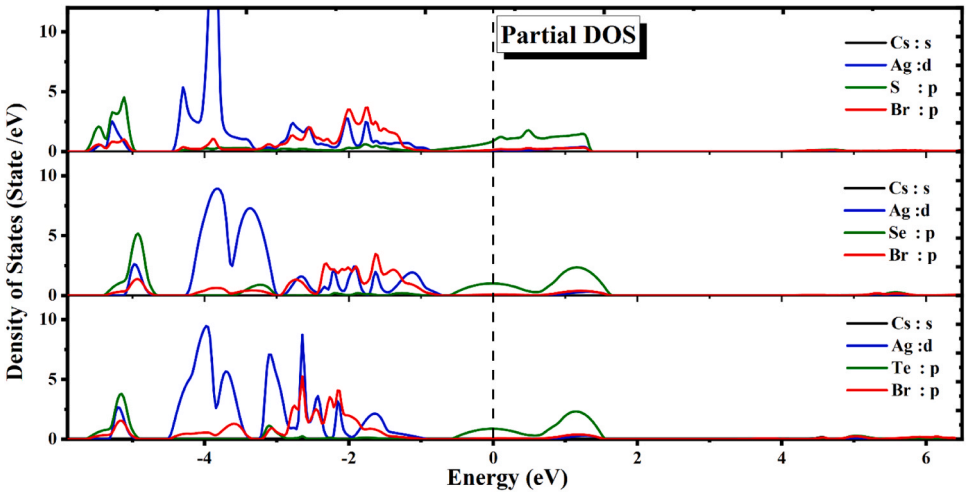

Fig. 4. The partial density of states (PDOS) of Cs_2AgXBi_6 compounds.

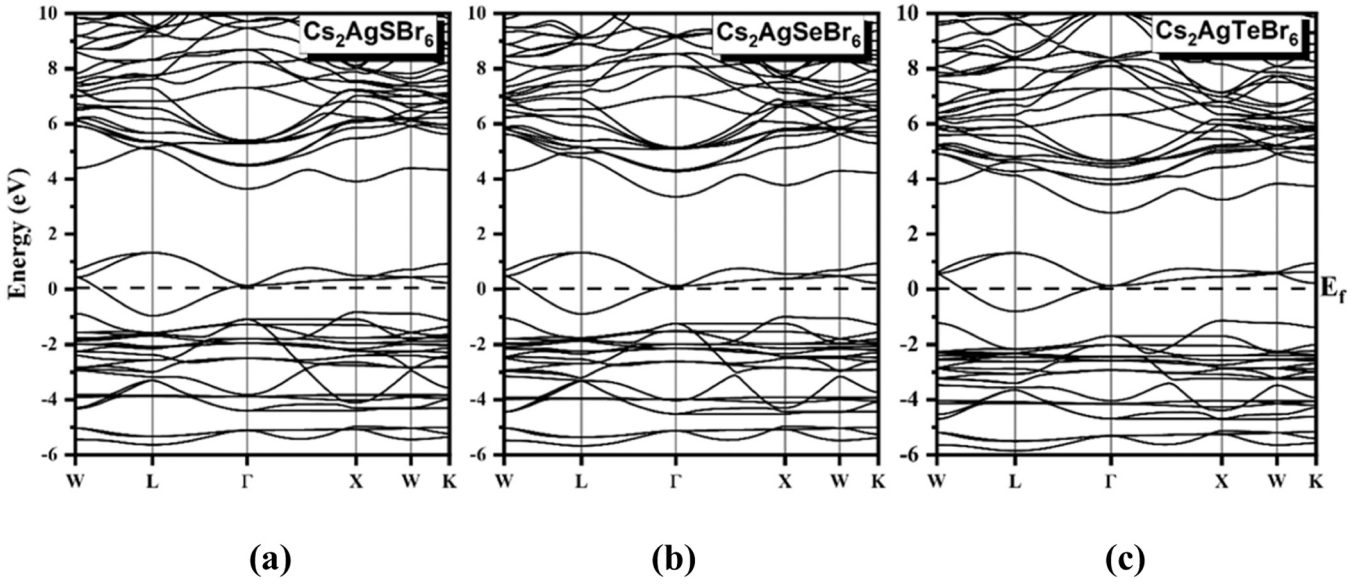

Fig. 5. The predicted band structure of Cs_2AgXBi_6 compounds where **(a)** X = S, **(b)** X = Se and **(c)** X = Te.

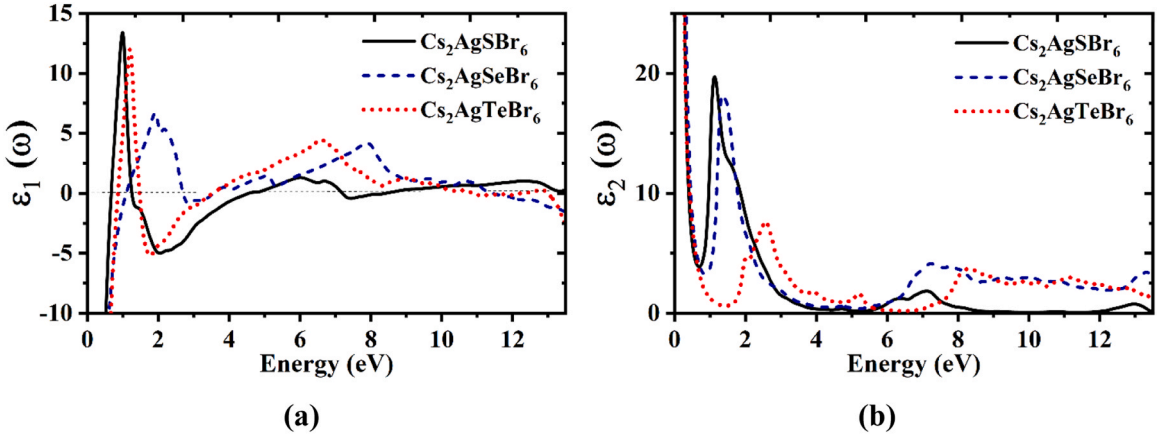

Fig. 6. **(a)** real (ε_1) and **(b)** imaginary (ε_2) parts of the complex dielectric function (ε) versus the energy of the incident photon.

regions for Cs_2AgXBr_6 indicates that the incident photons are attenuated due to the energy dissipation in the medium, resulting in a metallic behavior and zero dielectric behavior. The first maximum peak of the imaginary part ε_2 of the dielectric constant occurs at an energy less than 0.5 eV, which may be attributed to the cooperative behavior for both spins channels, in which the metallic phenomenon fluctuates the main peak to lower energy.

The optical conductivity of a material is a property that measures how much of an electric field can withstand while being subjected to an alternating-frequency electric field, and how much of an induced current can sustain as a result.

Fig. 7 depicts the variation of the real and imaginary parts of the optical conductivity for Cs_2AgXBr_6 compounds as a function of photon energy. In general, $Re(\sigma)$ behaves as expected, rising with increasing energy despite the presence of peaks. The average length of the high-energy peaks is shorter than that of the low-energy peaks in all compounds except Cs_2AgSBr_6. $Re(\sigma)$ peaks for Cs_2AgSBr_6 occur at 1.10, 7.08, and 13 eV, with the highest peak at 1.10 eV. $Cs_2AgSeBr_6$ has a maximum peak at 13.33 eV and peaks at 1.48, 7.28, 10.12, and 13.30 eV for $Re(\sigma)$. Furthermore, $Re(\sigma)$ for $Cs_2AgTeBr_6$ occurs at 2.61, 5.16, 8.35, and 11.07 eV, with the highest peak occurring at 11.07 eV. From Fig. 7(a), we can note that the real part of optical conductivity for $Cs_2AgSeBr_6$ and $Cs_2AgTeBr_6$ are similar, but it is different for Cs_2AgSBr_6. The physical origin of this difference is that the electronic configuration of the S, Se, and Te, since Se and Te have d state while S has not d state.

The $Im(\sigma)$ varies between positive and negative values, with maximum values of 2.44, 1.93, and 3.01 eV for Cs_2AgXBr_6 (X = S, Se, and Te) and minimum values of 12.41, 6.67, and 8.00 eV for the same compound arrangement.

Fig. 8 depicts the energy dependence of the absorption coefficient $I(\omega)$, the reflectivity $R(\omega)$, the transmittance, and the energy loss function $L(\omega)$. The amount of light absorbed by a material is expressed as its absorption coefficient, which is the amount of light per unit length in a medium. It also characterizes the rate at which electrons lose energy as they move through a material [26,36,58].

For $Cs_2AgSeBr_6$ and $Cs_2AgTeBr$ compounds, the absorption coefficient increases with increasing energy, while the reflectivity decreases. Corresponding to the transmittance of $Cs_2AgSeBr_6$ and $Cs_2AgTeBr$ compounds, these materials are semi-transparent in the visible region of the electromagnetic spectrum. For $Cs_2AgSeBr_6$, the maximum transmission occurs at 0.9 and 4.17 eV, while for $Cs_2AgTeBr_6$ it occurs at 1.23 and 6.06 eV. However, Cs_2AgSBr_6 have a transmittance in energy range 0–1.3, 3.05–7.04, and 7.79–13 eV. The calculated plasma frequency (ω_p) values, which corresponds to the lateral edge in the reflection spectra, of the Cs_2AgXBr_6 (X = S, Se, and Te) compounds are 2.56, 3.06, and 2.32 eV, respectively. For Cs_2AgSBr_6, light loss is minimal across the range from 0 to 4 eV (infrared and visible spectra). $Cs_2AgSeBr_6$ and $Cs_2AgTeBr_6$ have minimum loss value at 2 eV and from 6–8 eV, respectively.

Fig. 9 depicts the variation of the real $n(\omega)$ and imaginary $k(\omega)$ components of the complex refractive index as a function of energy. The refractive index refers to the real part, while the extinction coefficient refers to the imaginary part. Many photoelectric applications rely on the material's k(ω), making it an important optical property [59]. Both $n(\omega)$ and $k(\omega)$ show a negative correlation with energy, as shown in Fig. 9. Cs_2AgXBr_6 compounds exhibit nearly identical behavior for the optical constants n(ω) and $k(\omega)$. Fig. 9 shows that Cs_2AgSBr_6 has larger values of $n(\omega)$ and $k(\omega)$ in the infrared and visible regions than that for the $Cs_2AgSeBr_6$ and $Cs_2AgTeBr_6$ compounds. Cs_2AgXBr_6 compounds that have almost similar values of $k(0)$ (51.3, 47.2, 62.2, respectively). Furthermore, $n(0)$ values are approximately the same (44, 41, 54) for the $Cs_2AgSeBr_6$ and $Cs_2AgTeBr_6$. Cs_2AgXBr_6 compounds. The high refractive indexes indicate increased polarization because of interacting the incident photons with larger number of electrons. It should be noted that $n(0)$ and $\varepsilon_1(0)$ are related through the relation $n(0) = \varepsilon_1(0)$.

3.4. Thermodynamic properties

The heat capacities of the three compounds under investigation were determined using the Debye quasi harmonic model, which is incorporated into the GIBBS2 software. This analysis was conducted under varying pressures, reaching up to 15 GPa, and within a temperature range of up to 650 K. The results depicted in the Fig. 10 revealed distinct trends: firstly, the calculated heat capacity (C_v) values exhibited an exponential increase as the temperature rose when. Secondly, these values stabilized at a constant level starting from a temperature of 400 Kelvin. Conversely, it was observed that within a thermal range below 350 Kelvin, the heat capacity decreased as the pressure increased. This behavior can be attributed to the pressure's influence in reducing the degrees of freedom, particularly the vibrational modes of the atoms within the compounds.

This study offers valuable insights into how these compounds respond to variations in temperature and pressure, emphasizing the impact of pressure on molecular vibrations and its subsequent effect on heat capacity.

Entropy, represented as S, has dual physical depictions. Microscopically, it gauges a system's disorder with the equation $S = kln(\Omega)$, where Ω signifies the potential configurations. Elevated entropy signifies increased disorder and greater diversity in configurations. On the macroscopic scale, entropy measures the internal energy inaccessible for productive work, characterizing it as essentially non-convertible energy [60].

The dependence of entropy on heat and pressure for Sc2AgXBr6 (X = S, Se and Te) compounds, as illustrated in figure *, reveals that

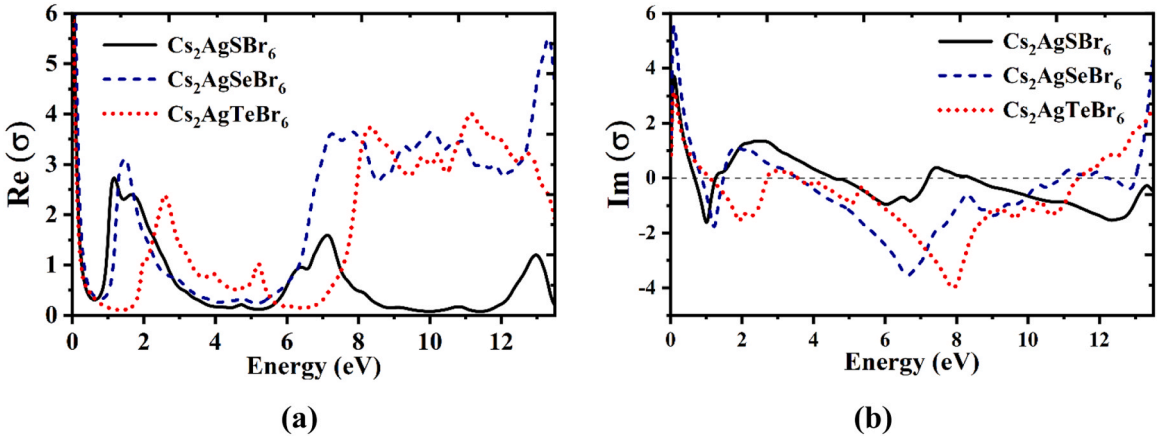

Fig. 7. **(a)** Real and **(b)** imaginary parts of the optical conductivity versus the energy of the incident photon.

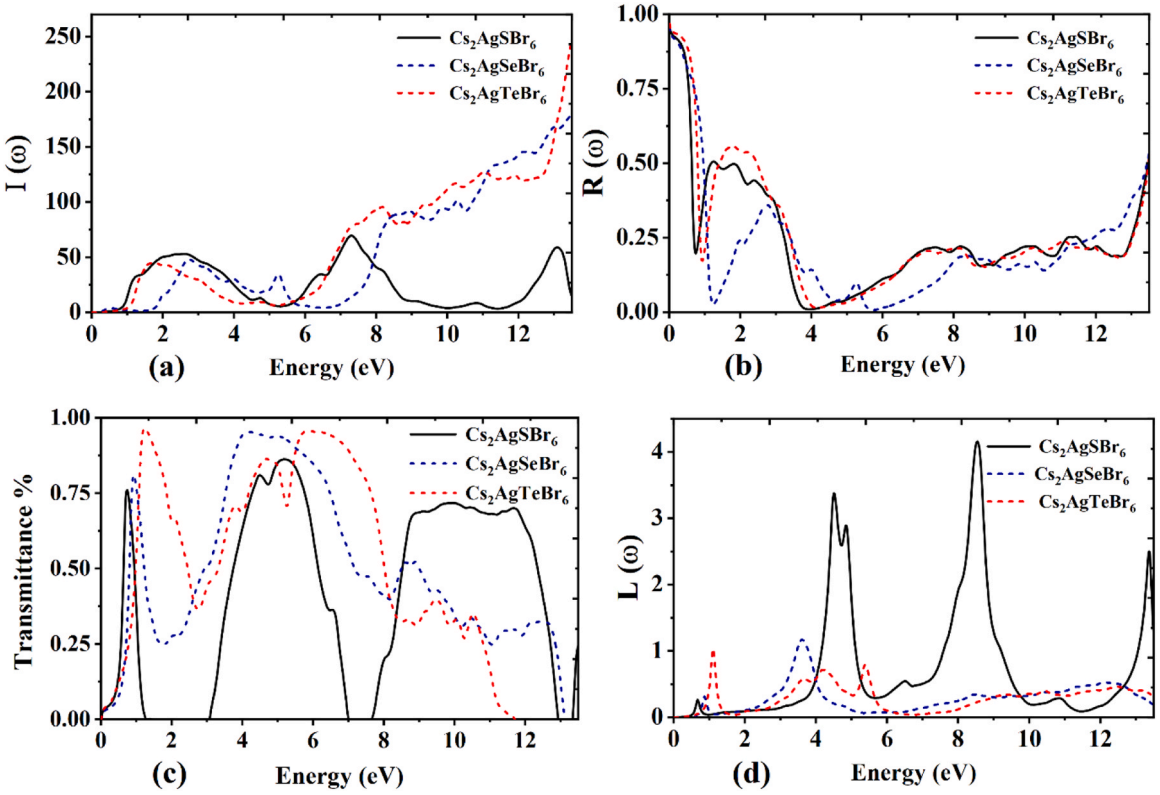

Fig. 8. **(a)** The absorption coefficient, **(b)** the reflectivity, **(d)** The Transmittance, and **(d)** the energy loss function versus the energy of the incident photon.

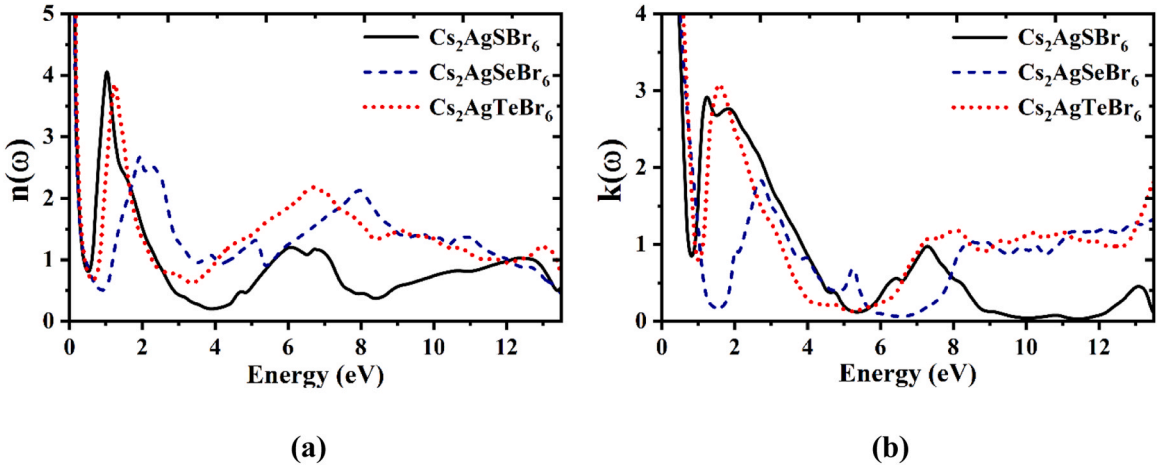

Fig. 9. **(a)** The refractive index n(ω) and **(b)** the extinction coefficient k(ω) versus the energy of incident photon.

entropy increases almost linearly with rising temperature, while it decreases inversely with the influence of pressure. This is attributed to the fact that pressure reduces the number of possible states for atomic vibration patterns, whereas heat tends to increase them. The Debye Temperature, which has multiple correlations with various physical properties of materials, was studied under the influence of temperature at constant pressures of 0, 5, 10, and 15 GPa. The Debye temperature expresses the highest heat value that the system can reach due to a single normal vibration [60]. The results obtained regarding this parameter indicate that the influence of temperature on Debye temperature is barely weak, whereas pressure has a significant effect. An application of pressure by a factor of 5 GPa is capable of raising the Debye temperature by approximately 90 K. Additionally, the findings suggest that the studied compounds exhibit low Debye temperatures, implying their characterization as "soft" materials.

The obtained values for the thermal expansion coefficients of the compounds Cs2AgXBr6 (X = S, Se, and Te) indicate that these compounds exhibit low values at low temperatures, increasing significantly with rising temperature until reaching 150 Kelvin. At this point, these compounds exhibit only slight expansion, giving them good volume stability against thermal changes at ambient temperature. Additionally, applying an external pressure of just 5 GPa reduces the thermal expansion coefficient to half its value without pressure. Furthermore, the results confirm that, at the same temperature and pressure conditions, the compound Sc2AgTeBr6 has a lower thermal expansion coefficient compared to the other two compounds.

The vibration of particles in crystalline compounds contributes to heat transfer. We calculated the thermal conductivity for the crystalline

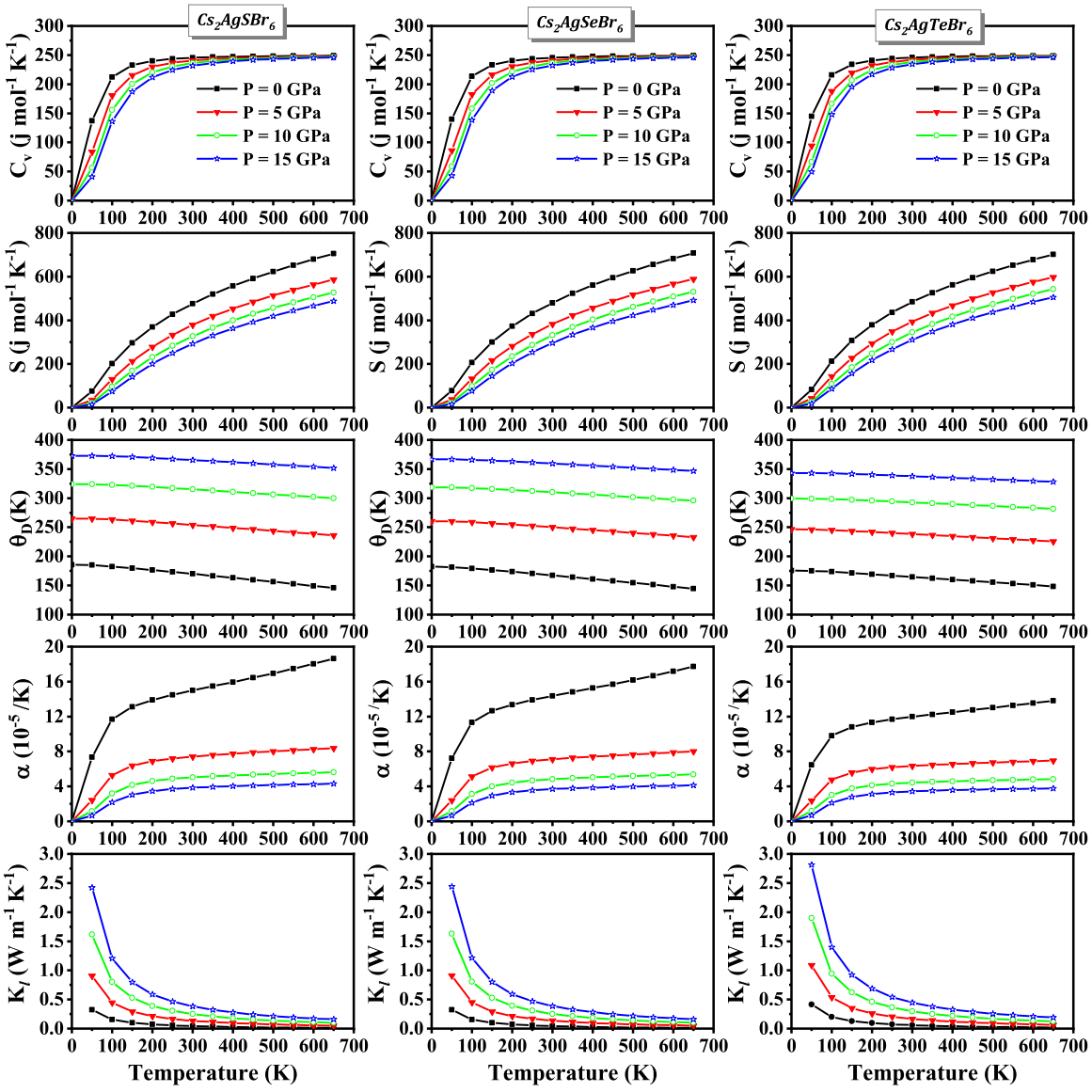

Fig. 10. The heat capacities (Cv), Entropy (S), Debye temperature (θ_D), Thermal expansion Coefficent (α) and thermal conductivity (K_l).

compounds under study. It became evident through the thermal conductivity-temperature curves that all three compounds exhibit very low thermal conductivity, not exceeding 0.7 $W.m^{-1} K^{-1}$ at zero pressure and temperatures below 100 K. However, these values increase with increasing pressure for temperatures not exceeding 100 K and converge towards a value of approximately 0.3 $W.m^{-1} K^{-1}$ at temperatures exceeding 350 K.

4. Conclusions

We have performed first-principles calculations on the structural, electronic, and optical properties of Cs_2AgXBr_6 (X = S, Se, and Te) double perovskite compounds. We investigated these new compounds in terms of their structural stability, the electronic and optical properties. The equilibrium structural and elastic parameters of $X_2AgBiBr_6$ show that these compounds are elastically stable, ductile, anisotropic, and ionically bonded. Both Poisson ratio and Pugh ratio imply that Cs_2AgXBr_6 (X = S, Te, Se) compounds are ductile. The calculated DOS and the electronic band structures of the investigated compounds point up that there is no bandgap due to the overlap between the conduction band and the valence band. Thus, these compounds have metallic behavior as the band gap tends to zero. We calculated the optical transmittance of the Cs_2AgXBr_6 compounds and discussed their transparent behaviors. According to the calculated optical transmission spectra of these compounds, $Cs_2AgSeBr_6$ and $Cs_2AgTeBr_6$ are semi-transparent in the visible region of the electromagnetic spectrum. Owing to their promising metallic and semi-transparent behaviors, they can be considered as potential candidates for use in solar cells and other optoelectronic devices that operate in the ultraviolet region of the spectrum.

CRediT authorship contribution statement

Al Aqtash Nabil: Writing – review & editing, Writing – original draft, Visualization, Supervision, Methodology, Investigation, Formal analysis, Data curation, Conceptualization. **Al-Reyahi Anas:** Writing – original draft, Formal analysis, Data curation, Conceptualization. **Al Azar Said:** Writing – review & editing, Software, Investigation, Conceptualization. **Essaoud Saber Saad:** Writing – original draft, Investigation, Data curation. **Maghrabi Mufeed:** Writing – review & editing, Writing – original draft, Supervision, Conceptualization. **Mufleh Ahmad:** Writing – original draft, Visualization, Data curation.

Ketfi Mohammed Elamin: Writing – original draft, Software, Data curation, Conceptualization. **Berarma Khadidja:** Writing – review & editing, Writing – original draft.

Declaration of Competing Interest

The authors declare that they have no known competing financial interests or personal relationships that could have appeared to influence the work reported in this paper.

Data availability

Data will be made available on request.

Acknowledgment

The financial support from The Hashemite University is gratefully acknowledged.

References

[1] P. Pistor, M. Meyns, M. Guc, H.-C. Wang, M.A.L. Marques, X. Alcobé, A. Cabot, V. Izquierdo-Roca, Advanced Raman spectroscopy of Cs2AgBiBr6 double perovskites and identification of Cs3Bi2Br9 secondary phases, Scr. Mater. 184 (2020) 24–29.
[2] L.M. Herz, Charge-carrier mobilities in metal halide perovskites: fundamental mechanisms and limits, ACS Energy Lett. 2 (2017) 1539–1548.
[3] L. Schade, A.D. Wright, R.D. Johnson, M. Dollmann, B. Wenger, P.K. Nayak, D. Prabhakaran, L.M. Herz, R. Nicholas, H.J. Snaith, P.G. Radaelli, Structural and optical properties of Cs_2 $AgBiBr_6$ double perovskite, ACS Energy Lett. 4 (2019) 299–305.
[4] T. Saha-Dasgupta, Double perovskites with 3d and 4d/5d transition metals: compounds with promises, Mater. Res Express 7 (2020) 014003.
[5] Z.-Y. Wang, Y. Chen, C. Zhang, D. Wang, P. Liang, H. Zhang, R.-J. Xie, L. Wang, Electronic structure and optical properties of vacancy-ordered double perovskites Cs_2 Pd Br_x Cl_{6-x} by first-principles calculation, J. Phys. Chem. C 124 (2020) 13310–13315.
[6] S. Vasala, M. Karppinen, A2B′B″O6 perovskites: a review, Prog. Solid State Chem. 43 (2015) 1–36.
[7] G. King, P.M. Woodward, Cation ordering in perovskites, J. Mater. Chem. 20 (2010) 5785.
[8] A. Kojima, K. Teshima, Y. Shirai, T. Miyasaka, Organometal halide perovskites as visible-light sensitizers for photovoltaic cells, J. Am. Chem. Soc. 131 (2009) 6050–6051.
[9] L.C. Andreani, A. Bozzola, P. Kowalczewski, M. Liscidini, L. Redorici, Silicon solar cells: toward the efficiency limits, Adv. Phys. X 4 (2019) 1548305.
[10] Q. Sun, H. Chen, W.-J. Yin, Do chalcogenide double perovskites work as solar cell absorbers: a first-principles study, Chem. Mater. 31 (2019) 244–250.
[11] A.H. Slavney, T. Hu, A.M. Lindenberg, H.I. Karunadasa, A Bismuth-Halide double perovskite with long carrier recombination lifetime for photovoltaic applications, J. Am. Chem. Soc. 138 (2016) 2138–2141.
[12] H. Chen, C.-R. Zhang, Z.-J. Liu, J.-J. Gong, W. Wang, Y.-Z. Wu, H.-S. Chen, Vacancy defects on optoelectronic properties of double perovskite Cs2AgBiBr6, Mater. Sci. Semicond. Process 123 (2021) 105541.
[13] J.-P. Correa-Baena, M. Saliba, T. Buonassisi, M. Grätzel, A. Abate, W. Tress, A. Hagfeldt, Promises and challenges of perovskite solar cells, Science 358 (*1979*) (2017) 739–744.
[14] N.-G. Park, Perovskite solar cells: an emerging photovoltaic technology, Mater. Today 18 (2015) 65–72.
[15] N. Wang, L. Zhan, S. Li, M. Shi, T.-K. Lau, X. Lu, R. Shikler, C.-Z. Li, H. Chen, Enhancement of intra- and inter-molecular π-conjugated effects for a non-fullerene acceptor to achieve high-efficiency organic solar cells with an extended photoresponse range and optimized morphology, Mater. Chem. Front. 2 (2018) 2006–2012.
[16] W. Gao, C. Ran, J. Xi, B. Jiao, W. Zhang, M. Wu, X. Hou, Z. Wu, High-quality Cs_2 $AgBiBr_6$ double perovskite film for lead-free inverted planar heterojunction solar cells with 2.2% efficiency, ChemPhysChem 19 (2018) 1696–1700.
[17] L. Dong, S. Sun, Z. Deng, W. Li, F. Wei, Y. Qi, Y. Li, X. Li, P. Lu, U. Ramamurty, Elastic properties and thermal expansion of lead-free halide double perovskite Cs2AgBiBr6, Comput. Mater. Sci. 141 (2018) 49–58.
[18] E.T. McClure, M.R. Ball, W. Windl, P.M. Woodward, Cs_2 $AgBiX_6$ (X = Br, Cl): new visible light absorbing, lead-free Halide Perovskite semiconductors, Chem. Mater. 28 (2016) 1348–1354.
[19] Y. Soni, U. Rani, A. Shukla, T.K. Joshi, A.S. Verma, Transition metal-based halides double Cs2ZSbX6 (Z = Ag, Cu, and X = Cl, Br, I) perovskites: a mechanically stable and highly absorptive materials for photovoltaic devices, J. Solid State Chem. 314 (2022) 123420.
[20] J. Su, T. Mou, J. Wen, B. Wang, First-principles study on the structure, electronic, and optical properties of Cs $_2$ AgBiBr $_{6-x}$ Cl $_x$ mixed-halide double perovskites, J. Phys. Chem. C 124 (2020) 5371–5377.
[21] G. Kresse, J. Furthmüller, Efficient iterative schemes for ab initio total-energy calculations using a plane-wave basis set, Phys. Rev. B 54 (1996) 11169–11186.
[22] G. Kresse, J. Furthmüller, Efficiency of ab-initio total energy calculations for metals and semiconductors using a plane-wave basis set, Comput. Mater. Sci. 6 (1996) 15–50.
[23] A.Y. Al-Reyahi, S. Al Azar, A.A. Mousa, S.S. Essaoud, M. Maghrabi, K. Berarma, A. Aqili, A. Mufleh, H.I. Abu Radwan, Investigation of electronic, optical, and thermoelectric properties of half-metallic spinel X2NO4 (X=B, Al): first-principles calculations, Comput. Condens. Matter 34 (2023) e00787.
[24] K. Berarma, S.S. Essaoud, A.A. Mousa, S.M. Azar, A.Y. Al-Reyahi, Opto-electronic, thermodynamic and charge carriers transport properties of Ta $_2$ FeNiSn $_2$ and Nb $_2$ FeNiSn $_2$ double half-Heusler alloys, Semicond. Sci. Technol. 37 (2022) 055013.
[25] Y.M. Odeh, S.M. Azar, A.Y. Al-Reyahi, A.A. Mousa, E.K. Jaradat, N. Al Aqtash, Tuning the bandgap of cubic and orthorhombic BaZrS3 by substituting sulfur with selenium, AIP Adv. 13 (2023).
[26] N. Aqtash, Al, S.M. Al Azar, A.Y. Al-Reyahi, A. Mufleh, M. Maghrabi, S.S. Essaoud, K. Berarma, A.A. Mousa, First-principles calculations to investigate structural, mechanical, electronic, optical, and thermoelectric properties of novel cubic double Perovskites X2AgBiBr6 (X=Li, Na, K, Rb, Cs) for optoelectronic devices, Mol. Simul. (2023) 1–12.
[27] M.E. Ketfi, S.S. Essaoud, S. Al Azar, A.Y. Al-Reyahi, A.A. Mousa, A. Mufleh, Insight into the spin-polarized structural, optoelectronic, magnetic, thermodynamic, and thermoelectric properties of PdBO2 (B = Al, Cr, and Rh) Delafossite semiconductor, Opt. Quantum Electron 55 (2023) 1013.
[28] J.P. Perdew, Jacob's ladder of density functional approximations for the exchange-correlation energy. AIP Conference Proceedings, AIP, 2001, pp. 1–20.
[29] P. Blaha, K. Schwarz, F. Tran, R. Laskowski, G.K.H. Madsen, L.D. Marks, WIEN2k: an APW+lo program for calculating the properties of solids, J. Chem. Phys. 152 (2020) 074101.
[30] K. Schwarz, DFT calculations of solids with LAPW and WIEN2k, J. Solid State Chem. 176 (2003) 319–328.
[31] C. Hébert, Practical aspects of running the WIEN2k code for electron spectroscopy, Micron 38 (2007) 12–28.
[32] D. Koller, P. Blaha, F. Tran, Hybrid functionals for solids with an optimized Hartree–Fock mixing parameter, J. Phys.: Condens. Matter 25 (2013) 435503.
[33] F. Tran, P. Blaha, Implementation of screened hybrid functionals based on the Yukawa potential within the LAPW basis set, Phys. Rev. B 83 (2011) 235118.
[34] A.D. Becke, E.R. Johnson, A simple effective potential for exchange, J. Chem. Phys. 124 (2006).
[35] F. Tran, P. Blaha, M. Betzinger, S. Blügel, Comparison between exact and semilocal exchange potentials: an all-electron study for solids, Phys. Rev. B Condens Matter Mater. Phys. 91 (2015).
[36] K. Berarma, S.S. Essaoud, A.A. Mousa, S.M. Azar, A.Y. Al-Reyahi, Opto-electronic, thermodynamic and charge carriers transport properties of Ta2FeNiSn2and Nb2FeNiSn2double half-Heusler alloys, Semicond. Sci. Technol. 37 (2022).
[37] A.Y. Al-Reyahi, S. Al Azar, A.A. Mousa, S.S. Essaoud, M. Maghrabi, K. Berarma, A. Aqili, A. Mufleh, H.I. Abu Radwan, Investigation of electronic, optical, and thermoelectric properties of half-metallic spinel X2NO4 (X=B, Al): first-principles calculations, Comput. Condens. Matter 34 (2023) e00787.
[38] D. Murnaghan B F 1915 *THE COMPRESSIBILITY OF MEDIA UNDER EXTREME PRESSURES* vol 18 (Univ. Texas Public).
[39] N. Mehmood, R. Ahmad, Structural, electronic, magnetic, and optical properties of half-heusler alloys RuMnZ (Z = P, As): a first-principle study, J. Supercond. Nov. Magn. 31 (2018) 233–239.
[40] Y.-Y. Yang, P. Gong, W.-D. Ma, R. Hao, X.-Y. Fang, Effects of substitution of group-V atoms for carbon or silicon atoms on optical properties of silicon carbide nanotubes, Chin. Phys. B 30 (2021) 067803.
[41] A.M. Mebed, M. Mushtaq, I. Muhammad, I.U.N. Lone, S. AL-Qaisi, N. Algethami, E. F. EL-Shamy, A. Laref, N.M. AL-Hosiny, Structure, half-metallic and magnetic properties of bulk and (001) surface of Rb 2 XMoO 6 (X = Cr, Sc) double perovskites: a DFT + U study, Phys. Scr. 98 (2023) 015807.
[42] A. Togo, I. Tanaka, First principles phonon calculations in materials science, Scr. Mater. 108 (2015) 1–5.
[43] A.Y. Al-Reyahi, A. Mufleh, S.M. Al Azar, M. Maghrabi, N. Al Aqtash, S.S. Essaoud, K. Berarma, A. Shaheen, M.E. Ketfi, A.A. Mousa, Exploring the physical properties of cubic CsGeBr3-nIn (n= 0, 1, 2, 3) compounds: Ab initio calculations of perovskites prospective for the application in solar cells, Solid State Sci. (2023) 107435.
[44] M. Maghrabi, A.Y. Al-Reyahi, N. Aqtash, Al, S.M. Al Azar, A. Shaheen, A. Mufleh, B. Shaban, Investigating the physical properties of lead-free halide double perovskites Cs2AgXBr6 (X = P, As, Sb) for photovoltaic and thermoelectric devices using the density functional theory, Mater. Today Commun. 37 (2023) 107541.
[45] J. Wang, S. Yip, S.R. Phillpot, D. Wolf, Crystal instabilities at finite strain, Phys. Rev. Lett. 71 (1993) 4182–4185.
[46] S. Al-Qaisi, D.P. Rai, T. Alshahrani, R. Ahmed, B.U. Haq, S.A. Tahir, M. Khuili, Q. Mahmood, Structural, elastic, thermodynamic, electronic, optical and thermoelectric properties of MgLu2×4 (X= S, Se) spinel compounds from ab-initio calculations, Mater. Sci. Semicond. Process 128 (2021).
[47] D.G. Pettifor, Theoretical predictions of structure and related properties of intermetallics, Mater. Sci. Technol. 8 (1992) 345–349.
[48] R. Hill, The elastic behaviour of a crystalline aggregate, Proc. Phys. Soc. Sect. A 65 (1952) 349–354.
[49] M.A. Hadi, Superconducting phases in a remarkable class of metallic ceramics, J. Phys. Chem. Solids 138 (2020) 109275.

[50] N. Arikan, G. DikiCi Yildiz, Y.G. Yildiz, A. İyigör, Electronic, elastic, vibrational and thermodynamic properties of HfIrX (X = As, Sb and Bi) compounds: insights from DFT-based computer simulation, J. Electron Mater. 49 (2020) 3052–3062.
[51] J. Wang, Y. Zhou, Dependence of elastic stiffness on electronic band structure of nanolaminate M2AlC (M=Ti,V,Nb, and Cr) ceramics, Phys. Rev. B 69 (2004) 214111.
[52] S.F. Pugh, XCII. Relations between the elastic moduli and the plastic properties of polycrystalline pure metals, The London, Edinburgh, and Dublin Philosophical Magazine and Journal of Science 45 (1954) 823–843.
[53] A.A. Mousa, S. Al-Qaisi, M. Abu-Jafar, S. Al Azar, R. Jaradat, J.M. Khalifeh, T. Ouahrani, R. Khenata, Ab initio studies of the structural, elastic, electronic and optical properties of the Ni3In intermetallic compound, Mater. Chem. Phys. 249 (2020).
[54] R. De, L. Kronig, On the theory of dispersion of x-rays, Opt. Soc. Am. vol 12 (1926).
[55] H. Wang, Y. Chen, Y. Kaneta, S. Iwata, First-principles study on effective doping to improve the optical properties in spinel nitrides, J. Alloy. Compd. 491 (2010) 550–559.
[56] Chu C.W., Chen F., Shulman J., Tsui S., Xue Y.Y., Wen W. and Sheng P. 2005 A negative dielectric constant in nano-particle materials under an electric field at very low frequencies *Strongly Correlated Electron Materials: Physics and Nanoengineering* vol 5932 (SPIE) p 59320X.
[57] John David Jackson 1998 Classical Electrodynamics.
[58] M. Arbi, N. Benramdane, Z. Kebbab, R. Miloua, F. Chiker, R. Khenata, First principles calculations of structural, electronic and optical properties of zinc aluminum oxide, Mater. Sci. Semicond. Process 15 (2012) 301–307.
[59] J. Sun, X.F. Zhou, Y.X. Fan, J. Chen, H.T. Wang, X. Guo, J. He, Y. Tian, First-principles study of electronic structure and optical properties of heterodiamond BC2 N, Phys. Rev. B Condens Matter Mater. Phys. 73 (2006).
[60] S. Säad Essaoud, S.M. Al Azar, A.A. Mousa, R.S. Masharfe, Characterization of structural, dynamic, optoelectronic, thermodynamic, mechanical and thermoelectric properties of AMgF 3 (A = K or Ag) fluoro-perovskites compounds, Phys. Scr. 98 (2023) 035820.